Biomed Microdevices (2017) 19:10
DOI 10.1007/s10544-017-0151-x

Evidence of differential mass change rates between human breast cancer cell lines in culture

Elise A. Corbin[1,2,3] · **Olaoluwa O. Adeniba**[1,2] · **Olivia V. Cangellaris**[2,4] · **William P. King**[1,2] · **Rashid Bashir**[2,4]

Abstract Investigating the growth signatures of single cells will determine how cell growth is regulated and cell size is maintained. The ability to precisely measure such changes and alterations in cell size and cell mass could be important for applications in cancer and drug screening. Here, we measure the mass growth rate of individual benign (MCF-10A), non-invasive (MCF-7), and highly-invasive malignant (MDA-MB-231) breast cancer cells. A micro-patterning technique was employed to allow for the long-term growth of motile cells. Results show mass growth rates at 4.8%, 1.2%, and 2.8% for MCF-10A, MCF-7, and MDA-MB-231, demonstrating that normal cells have a higher mass growth rate than cancerous cells. All the cell lines show an increase in mass change rate indicating that the mass accumulation rate is exponential over a single cell cycle. The growth rates measured with our MEMS sensor are compared with doubling times obtained through conventional bulk analysis techniques, and exhibit excellent agreement.

Electronic supplementary material The online version of this article (doi:10.1007/s10544-017-0151-x) contains supplementary material, which is available to authorized users.

✉ Rashid Bashir
rbashir@illinois.edu

[1] Department of Mechanical Science and Engineering, University of Illinois Urbana-Champaign, Urbana, IL 61801, USA

[2] Micro and Nanotechnology Laboratory, University of Illinois Urbana-Champaign, Urbana, IL 61801, USA

[3] Perelman School of Medicine, University of Pennsylvania, Philadelphia, PA 19104, USA

[4] Department of Bioengineering, University of Illinois Urbana-Champaign, Urbana, IL 61801, USA

Keywords MEMS mass sensor · Breast cancer · Cell growth rate · Cell micromechanics · Resonant frequency

1 Introduction

Cell growth is necessary for life, but the mechanisms that control the regulation of cell mass, volume and growth rate are still poorly understood (Lloyd 2013; Zangle and Teitell 2014). Cancer arises from a number of mutations in the genetic makeup of a cell; through the cell cycle the mutated genetic makeup is transferred to daughter cells and proliferation causes these cells to multiply (Lodish et al. 2003; Alberts et al. 2002; Weinberg 2006).

Currently, a great deal is known about the consequences of the mutations, but on a fundamental level there is still much to learn. Cancerous mutations alter relevant signaling pathways, which in-turn influence the interaction and response of a cell to mechanical stimuli and growth factors, cell fate, proliferation, transcription, migration, or differentiation. These pathways can change how the cell cycle is regulated. In cancer, cells exhibit unregulated growth and division as a consequence of disrupted checkpoints within the cell cycle, which is triggered by the loss of proper signaling cues (Hanahan and Weinberg 2000, 2011).

Cell growth consists of coordinated changes in both mass and volume. A standard approach to measuring cell growth is through accurate monitoring of cell size. A Coulter counter is a well-established technique to measure cell volume and has deepened our understanding as to how cells regulate growth. However, cell mass is a more direct and precise indicator of cell size and it is more closely indicative of biosynthetic processes in a cell. There are many different approaches for measuring cellular growth

Published online: 31 January 2017

and there is a debate as to whether looking at an aggregate population is more correct and necessary (Cooper 2006; Mitchison 2003; Mitchison 2005). When dealing with time-dependent measurements, it is known that studying bulk properties will often overlook single cell events and provide misleading analysis (Di Carlo et al. 2012; Di Carlo and Lee 2006). Measuring the growth of single cells has many challenges to overcome (Popescu et al. 2014), including the ability to handle and manipulate individual cells in real time. However, the use of microelectromechanical systems (MEMS) has provided opportunities to make significant advances (Bryan et al. 2010; Son et al. 2012). Several precise MEMS measurement techniques have been recently developed to better understand how the biophysical properties of a cell affect its cycle progression and behavior in disease. This includes magnetic twisting cytometry (Wang and Thampatty 2006), optomechanical measures (Park et al. 2015), micropipette aspiration (Evans and Yeung 1989; Hochmuth 2016; Sato et al. 2016), quartz crystal microbalance (QCM) (Li et al. 2005), atomic force microscopy (AFM) (Cross et al. 2007; Kuznetsova et al. 2007; Plodinec et al. 2012), suspended microchannel resonator (SMR) (Son et al. 2012), and quantitative phase microscopy (QPM) (Popescu et al. 2008). Although QPM methods are widely used to study adherent cells, they can only measure the 'dry mass' of live cells; thus, they rely on a refractive index difference to measure the non-aqueous (proteins, nucleic acids, and lipid molecules) mass density of the cell. Meanwhile, allowable sample sizes in QCM are based on electrode dimensions, which limit its adoption. SMR uses a flow-through technique that senses the 'buoyant mass' of a cell – the volumetric difference between the densities of a cell and that of the media replaced by the cell – which is similar to the optically measured 'dry mass' as described in QPM. This limits the types of cells able to be studied with SMR. As an alternative to these methods, our pedestal resonant sensor measures the whole cell apparent mass and thus could potentially illustrate critical elements of cell growth.

In this paper, we use our MEMS resonant mass sensors to compare the long-term growth of benign epithelial cells (MCF-10A) with cancer cells of both high (MDA-MB-231) and low invasive properties (MCF-7). In order to measure long-term growth, we confine and trap single cells on the pedestal of the MEMS sensor and repeatedly observe its resonant frequency to explore the way that cells accumulate mass, grow, and divide. This approach is aided by the use of cell patterning on the suspended resonant devices in order to maintain capture of the cells over time (Corbin et al. 2014a). From this approach, we find that all the cell lines examined exhibit a growth rate that increases with cell mass, but that each cell line exhibits its own unique mass change rate.

2 Experimental methods

2.1 MEMS resonant pedestal sensor

The MEMS resonant mass sensor comprises four beam-springs suspending a square platform ($60 \times 60\ \mu m^2$), as has been described previously (Corbin et al. 2014b; Millet et al. 2012; Park et al. 2010). The pedestal design both allows for a large cell capture region and also minimizes the variation of the displacement amplitude across the vibrating platform to provide uniform mass sensitivity. These sensors are arrayed on a chip in a 9×9 format of 81 sensors to maximize throughput and capture efficiency. It operates in a first resonance mode for mass sensing, which is a vertical displacement vibration with resonant frequencies of approximately 160 *kHz* in air and 60 *kHz* in liquid. This sensor is driven by passing an actuation current through the sensor in a static magnetic field to generate a Lorentz force that forces vibration.

2.2 Micro-patterned surface functionalization

In order to improve cell capture and retention, cells are micro-patterned on the pedestal sensors through a selective functionalization and backfill passivation technique (Corbin et al. 2014a, b). First, a hydrophobic layer of hexamethyldisilizane (HMDS) was applied to the sensor surface through vapor deposition to promote efficient deposition of Pluronic® F127 (Dorvel et al. 2010). Due to the delicate nature of the structure, a photoresist transfer technique (Yeom and Shannon 2010) was used to provide a uniform layer of photoresist to be patterned. The sample was then developed and exposed to oxygen plasma to remove HMDS from the openings in the photoresist for deposition of collagen type I. After rinsing the surface with PBS, the chip was soaked in acetone to lift-off the photoresist, leaving collagen selectively on the pedestals of the sensors and surrounded by HMDS everywhere else. At this point, pluronic was deposited on the HMDS covering the beam springs and a thin edge of the pedestal sensor through a backfill technique. This has the effect of selectively promoting cell adhesion on the collagen-functionalized pedestal while blocking unwanted adhesion at sites with pluronic.

2.3 Cell mass measurement

The mass measurement procedure involves comparing the resonant frequency of a loaded sensor with its original, unloaded state to determine the mass of the loaded object. This is a well-characterized method described fully elsewhere (Corbin et al. 2013; Millet et al. 2012), therefore it will only be briefly introduced here. The measurement system combines electromagnetic actuation, a lock-in amplifier, and a laser

Doppler vibrometer (LDV) to measure the velocity of the vibrating MEMS sensor platform to ultimately determine the resonant frequency of the device. This is achieved by monitoring the difference in phase between applied actuation current and sensor vibration. The excitation frequency is updated based on this phase until converging upon the resonant frequency. This procedure is used to estimate the resonant frequency of the devices in a series of different states to extract the mass of the adhered cell.

Calculating object mass requires three separate resonant frequency measurements. First, the empty sensor resonant frequency was measured in air to obtain the spring constant. Next, the micro-patterning procedure was completed by backfilling with pluronic to passivate the remaining chip surfaces. We then placed a PDMS chamber over the sensor area, added fresh warm complete cell culture media, and sealed the chamber with a sterile glass coverslip. The sensor was then loaded into the incubation chamber of our system and allowed to stabilize to 37 °C prior to the measurement. The second empty sensor frequency was then measured in liquid to determine the reference frequency, which is reduced from the in-air frequency due to hydrodynamic loading. At this point cells were randomly seeded on the sensor area and allowed to attach for 1 h before being gently rinsed to remove non-adhered cells. The sensor is then restabilized at 37 °C in the incubation chamber with the necessary conditions for each cell type (i.e. humidity and CO_2 level). Finally, the in-liquid resonant frequency of the mass loaded sensors were measured for comparison with the empty reference sensor frequency to calculate the attached mass. This measurement of the loaded sensor frequency was repeated over time to produce a growth profile. Previous studies (Sato et al. 2016) show that through 250 in-media measurements, the sensor resonant frequency can be determined within ±0.94 Hz (95% Confidence Internal (CI)), yielding a mass resolution of 8.5 pg within a confidence interval of 95% in liquid. With this sensor mass resolution percentage of ~1% of a typical mammalian cell mass (~1 ng), we can guarantee that within a CI = 95%, an exponential and linear growth model can be differentiated by our resonant mass sensor (See Supplemental Information).

2.4 Breast epithelial cell culture

Normal human breast epithelial cells (MCF-10A) were cultured in Dulbecco's Modified Eagle Medium/Ham's F-12 (Gibco) with 5% horse serum, 20 ng/mL EGF, 0.5 mg/mL hydrocortisone, 100 ng/mL cholera toxin, 10 μg/mL insulin, and 1% penicillin streptomycin. Human breast adenocarcinoma cells (MCF-7) were cultured in Dubecco's Modified Eagle Medium (Gibco) with 10% fetal bovine serum and 1% penicillin streptomycin. Highly metastatic human breast adenocarcinoma cells (MDA-MB-231) were cultured in Leibovitz's

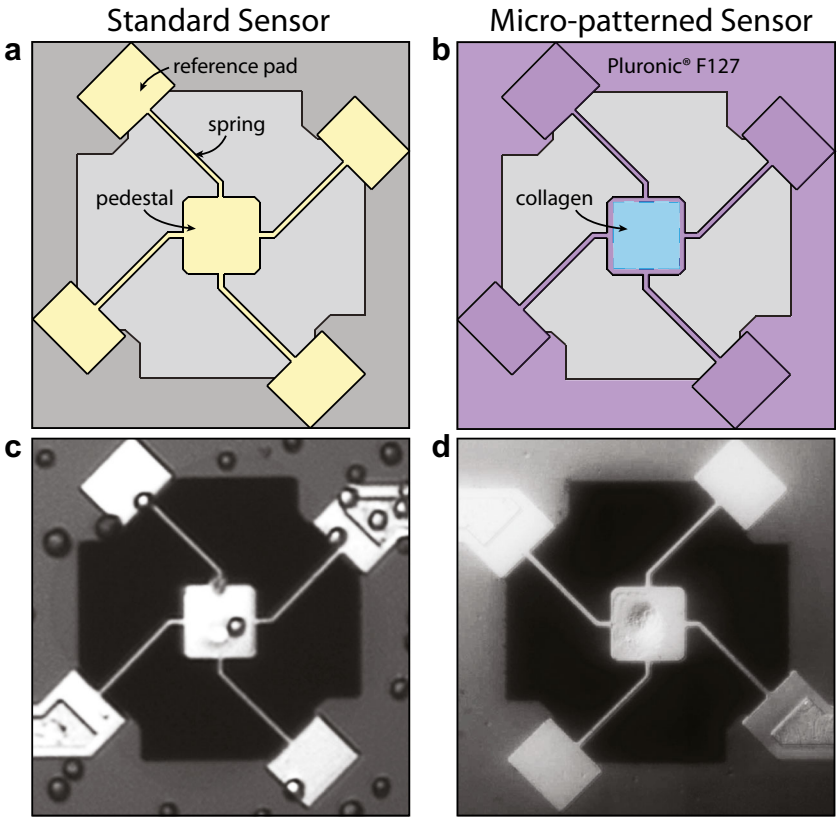

Fig. 1 Overview of sensor design with select functionalization and passivation: **a** Cartoon of the sensor layout; and **b** cartoon of the desired patterning with collagen selectively patterned in the center of the pedestal and with pluronic backfilled everywhere else **c** Bright field image of a single released non-patterned pedestal sensor that has been seeded with human colon cancer cells (HT29). It is shown that cells are able to attach to the springs and anywhere else that could ultimately compromise the cell measurement. **d** Bright Field image of a single released patterned pedestal sensor seeded with human breast cells (MCF-10A) and then rinsed to remove non-attached cells, leaving only the cell captured on the platform

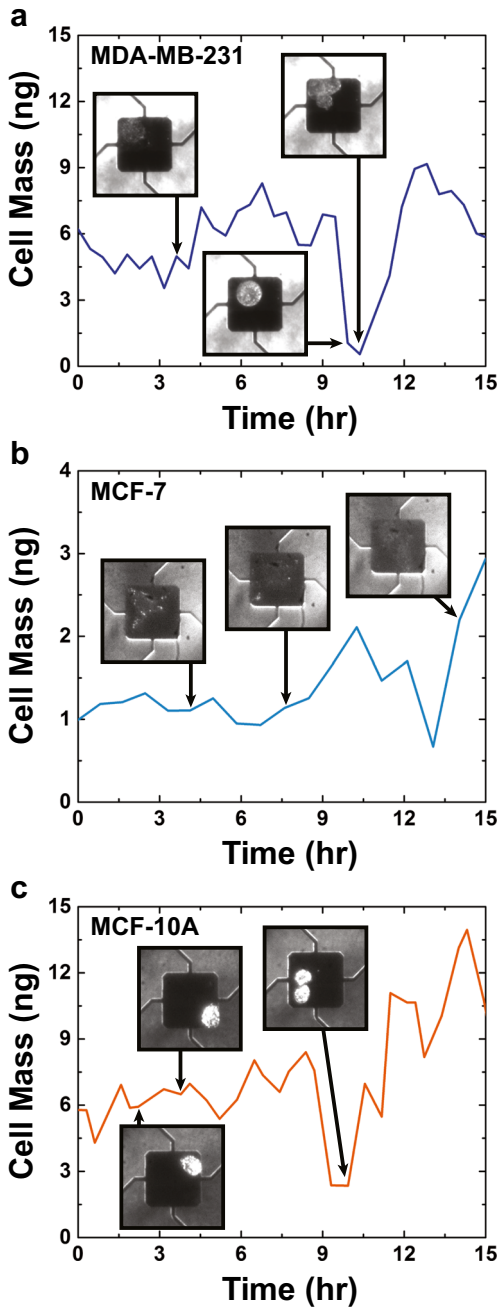

Fig. 2 Mass measurement of adherent cells versus time for each cell line: **a** MDA-MB-231; **b** MCF-7; and **c** MCF-10A. Each growth profile shows an increase of a single adherent cell, then will go through a cell division that is marked by a sudden decrease in cell mass, once division has completed, the growth profile continues

L-15 Medium (Sigma-Aldrich) with 10% fetal bovine serum and 1% penicillin streptomycin. MCF-7 and MCF-10A were cultured at 5% CO_2, 100% humidity, while MDA-MB-231 were cultured at 100% humidity and no CO_2.

Cells were introduced onto the sensors at a total of 9000 cells per chip and allowed to adhere. The sensors were rinsed with fresh growth media and the culture chamber was sealed with a sterilized glass cover slip for the measurement. Mass measurements were taken approximately every 20 min for up to 24 h.

2.5 Bulk doubling time measurements

Since cell-collagen interaction can strongly change cellular behavior, we performed doubling time experiments on collagen coated plastic dishes and non-collagen coated dishes for reference. We plated the all the cell lines at the same starting density of 318 cells/mm^2 and culture conditions as with the single cell analysis experiments and imaged them for 24 h. Using ImageJ we determined the cell count and found that MCF-7, MCF-10A, and MDA-MB-231 had doubling times of 43.7 ± 7.4, 20.1 ± 1.9, and 26.7 ± 8.8, respectively.

3 Results and discussion

Direct, long-term growth profiles of breast epithelial cell lines are measured using MEMS resonant pedestal sensors with micro-patterned surfaces for selective functionalization and passivation (Fig. 1). The cell lines studied include MDA-MB-231 and MCF-7, which are cancerous with high and low invasive potential, respectively, and a benign cell line, MCF-10A, for comparison. Repeated mass measurements of single cells captured on the mass sensor reveal the increase of cellular mass due to growth over the cell cycle. Figure 2 shows examples of individual cell growth curves that continue until the cell division where, interestingly, a temporary sharp decrease in apparent mass is detected (Movie S1-S3; Online Resource 1–3). These sharp decreases in apparent mass can be seen in the selected growth profiles at approximately 10, 13, and 9 h for MDA-MB-231, MCF-7, and MCF-10A, respectively; however, each investigated cell divided at a different time as our populations were not synchronized. During mitosis the dividing cell will partially detach from the platform, thus decreasing the contact area and altering the shape of the cell (Park et al. 2010). This geometry change can lead to a reduction of the inertial loading of the cell decreasing the apparent mass as described by a 2-DOF model (Corbin et al. 2015; Corbin et al. 2013; Park et al. 2010; Corbin et al. 2016). The result of the 2-DOF model revealed that geometry and viscoelasticity of the target, or cell, influences the mass measurement. Cells are known to be soft and cancer cells are known to be even softer (Cross et al. 2007; Guck et al. 2016; Wirtz et al. 2011). The viscoelastic properties of cells can lead to the cell operating out of phase with our sensor causing a geometry change of the cell. However, it is important to note that the increase in apparent mass during the cell growth represents a true increase in cell mass and is not a geometry or contact area artifact (Park et al. 2010).

To better investigate the growth dynamics of the benign and cancerous epithelial cell populations, we analyzed the

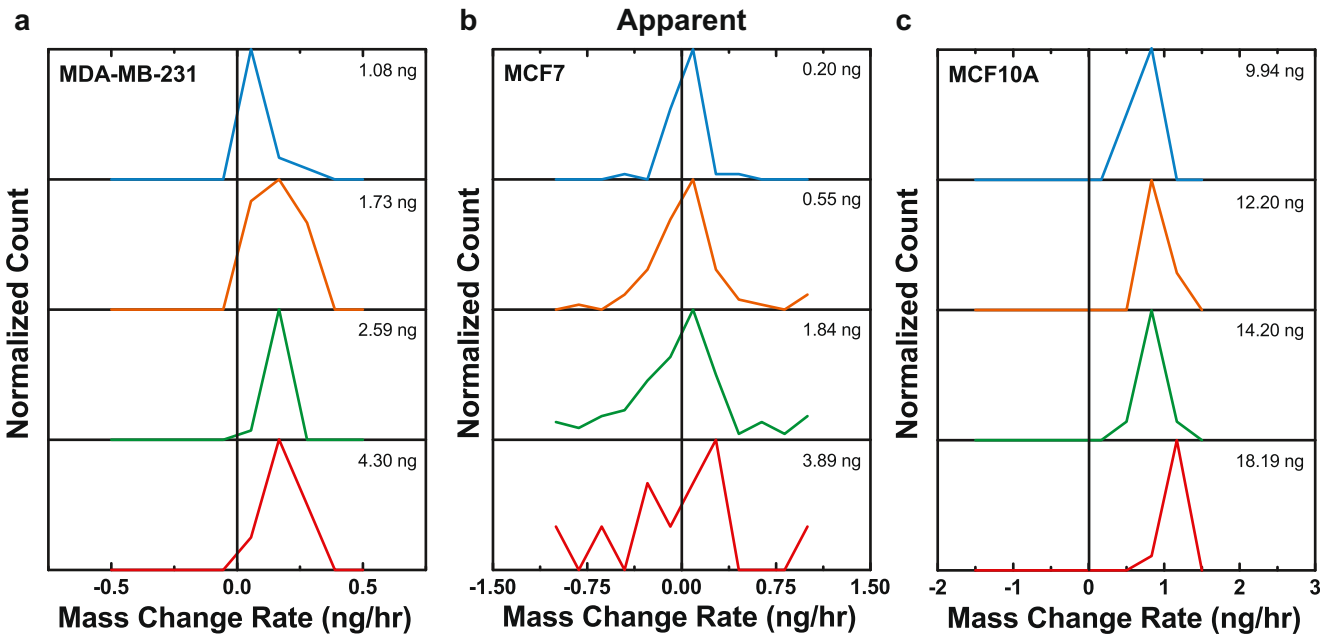

Fig. 3 Analysis of cell growth rate and mass change rate versus mass. Four histograms accounting for the mass accumulation at specific mass values: **a** MDA-MB-231; **b** MCF-7; and **c** MCF10-A

individual temporal mass profiles of all the cell lines. The derivative of the cell mass profiles provides the instantaneous mass change rate. For a given cell line, the data from each individual measured cell is pooled together, and Fig. 3 (a - c) show histograms of the instantaneous mass change rate data divided into four groups based on their instantaneous mass. It is clearly evident from these histograms that mass change rate does depend on the instantaneous cell mass. The small oscillations in mass data observed in Fig. 2 are expected and can lead to negative mass change rates. These oscillations can arise from a combination of short-term variations in cell viscoelasticity, density, or adhesion of the cell over the cell cycle. Small fluctuations of these properties occur naturally and have a small impact on the apparent mass detected by our sensors.

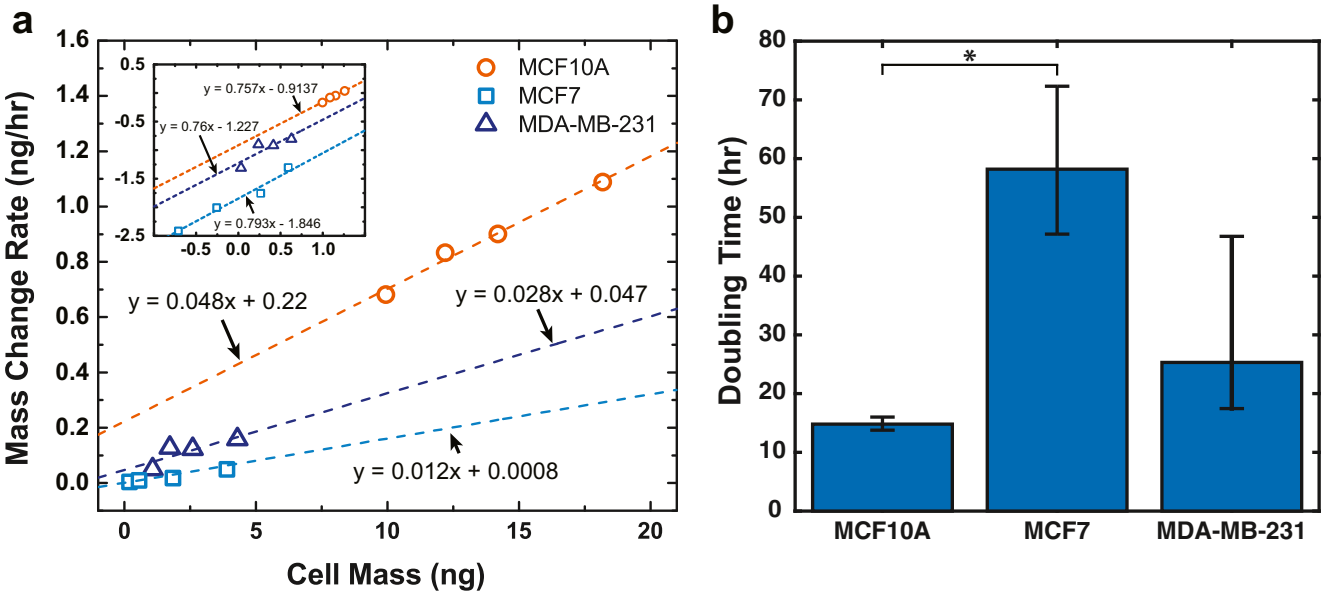

Fig. 4 Analysis of mass change rate per unit mass of individual cells. A five point moving average of changes in mass from all culture data points of individual breast cells. **a** Apparent values: Average cells acquire 1.2%, 2.8%, 4.8% additional mass every hour for MCF-7, MDA-MB- 231, and MCF-10A, respectively. (Inset) Log-log plot shows a power law of the different cell lines where the slopes are less than unity verifying consistency with scaling rules of energy consumption versus size of an organism. **b** Average doubling times found through mass measurement for MCF-7, MDA-MB- 231, and MCF- 10A with *error bars* representing standard error

Table 1 A comparison of the doubling times of the values obtained from the MEMS resonant sensor growth measurements and the American Type Culture Collection (ATCC) database values

Cell line	Doubling time		
	Measured (h)	Counted (h)	ATCC (h)
MCF-10A	14.8	20.1	16
MCF-7	58.2	43.7	38
MDA-MB-231	25.1	26.7	38

Despite these mass fluctuations, there is a clearly identifiable increase in cell mass over long periods of time, as confirmed by simultaneous optical imaging.

Fig. 4a translates the distributions found in Fig. 3 to find the cell mass growth rate indicated by the linear trends of the bin max peaks for both the apparent and corrected masses. These trends suggest that cells with greater mass also have an increased rate of mass accumulation, regardless of cell line. However, the cell lines do have different exponential growth rates, which is the slope of the mass change rate against mass. Figure 4a shows that MCF-10A, MCF-7, and MDA-MB-231 on average accumulate 4.8%, 1.2%, and 2.8% of their mass every hour for the apparent mass values. Figure 4b presents how the growth rates translate to mass doubling times of 14.8, 58.2, and 25.1 h ($= \log(2)/\log(1 + rate)$). To determine if doubling times measured with the sensor differed between cell lines, we used analysis of covariance (ANCOVA) to compare the fitted mass change rates. Through this analysis we found that the mass change rate, and thus the doubling time, significantly depended on cell line ($p = 0.012$). Post hoc tests between each cell line, with Bonferroni correction for multiple comparisons, found that MCF-7 and MCF-10A differed significantly ($p = 0.013$), but neither differed from MDA-MB-231 significantly ($p = 0.434$ for MCF-7 and $p = 0.182$ for MCF-10A). The inset of Fig. 4a presents log-log plots comparing mass change rate with cell mass. The growth follows the rules of scaling energy consumption by having a slope less than unity(Hou et al. 2008).

The American Type Culture Collection biological resource center (ATCC) provides doubling times, or the times for culture to double in size, for each cell line. For comparison, a population doubling time was considered for each cell line. In these bulk population experiments we recreated the microenvironment of our single cell experiments by coating collagen on plastic dishes. Table 1 collects the doubling time data of each cell line determined by ATCC, our population experiment, and our mass measurements. The MCF-10A cells appear to agree well with the bulk doubling time from ATCC, while they tend to grow slightly faster compared to our bulk doubling time measurements. The low invasive MCF-7 cells grow more slowly than the ATCC doubling times and our bulk doubling times. MDA-MB-231 (high invasive) cancer cell line agrees well between our measured and our bulk doubling times, however, it exhibits fairly substantial differences between measured and ATCC values. The differences in growth values are based on the direct measurement of mass of individual cells while both population and ATCC values are based on bulk cell counting. Although ATCC is a world reference for cell lines, the growing rate for each cell line varies with culture media and methodology. Heterogeneity exists within a homogeneous population implying that cells are not created equal, and yielding differences between cells such as size or mass. Expression of subtle signature differences in growth among individual cells can help explain why one cell may grow differently or lead to metastasis. Our measurements show good agreement with our bulk measures; however, a more in depth statistical analysis is necessary to verify differences between cell lines.

Recently, a deeper understanding of cell growth dynamics has revealed how cells grow individually and as a population over time (Park et al. 2010). This work has expanded upon that initial finding and validates it through the study of multiple cell lines. Here, we showed that the average growth rates of the investigated adherent cell lines increase with cell mass. It has been hypothesized that size homeostasis can be maintained in one of two ways: through linear growth without regulation (Conlon and Raff 2003), or exponential growth that requires check-point regulations (Godin et al. 2010; Tzur et al. 2009). While the specific regulatory factors defining growth are still intangible, it is likely that size is maintained by some signaling, possibly from environmental cues or genetics; however, we observe common trends between different cell lines that are consistent with previous findings (Park et al. 2010).

4 Conclusion

This paper presents the use of MEMS resonant sensors to investigate the differences in growth between benign and malignant adherent cancer cells through long-term mass measurements. Cells from each investigated cell line show an increase in mass change rate with respect to mass; therefore, the heavier cells accumulate more mass more quickly. Through the measurements with the MEMS sensor, we were able to determine that doubling time significantly depends on cell type, suggestive of inherent differences in cell growth depending on cancer phenotype. These doubling times also agreed well with bulk measurements and standard reference values from ATCC. The agreement in doubling time measures supports the accuracy of mass measurements, and future studies can take advantage of these devices to explore instantaneous growth of individual cells.

These measures have the ability to expand our understanding of adherent cell growth using a non-destructive technique capable of long-term observations. There are many highly regulated processes during cell growth including the replication of intracellular material that lead to mass accumulation, an increase in the physical size of the cell, and progression through the cell cycle. Through direct measurement of individual cell mass, we can better understand the mechanisms that form the basis of uncontrolled proliferation in cancer. The potential to expand the current system to include the monitoring of cell cycle status through optical verification with fluorescence promises a next generation of mass measurement for identification of growth rates during specific cycle phases.

References

B. Alberts, A. Johnson, J. Lewis, M. Raff, K. Roberts, P. Walter, *Molecular Biology of the Cell*, 4th edn. (Garland Science, New York, 2002)

A.K. Bryan, A. Goranov, A. Amon, S.R. Manalis, Proc. Natl. Acad. Sci. **107**, 999 (2010)

I. Conlon, M. Raff, J. Biol. **2** (2003)

S. Cooper, Theor. Biol. Med. Model. **3**, 10 (2006)

E.A. Corbin, L.J. Millet, J.H. Pikul, C.L. Johnson, J.G. Georgiadis, W.P. King, R. Bashir, Biomed. Microdevices. **15**, 311 (2013)

E.A. Corbin, B.R. Dorvel, L.J. Millet, W.P. King, R. Bashir, Lab Chip **14**, 1401 (2014a)

E.A. Corbin, L.J. Millet, K.R. Keller, W.P. King, R. Bashir, Anal. Chem. **86**, 4864 (2014b)

E.A. Corbin, F. Kong, C.T. Lim, W.P. King, R. Bashir, Lab Chip **15**, 839 (2015)

E.A. Corbin, O.O. Adeniba, R.H. Ewoldt, R. Bashir, Appl. Phys. Lett. **108**, 93701 (2016)

S.E. Cross, Y.-S. Jin, J. Rao, J.K. Gimzewski, Nat Nano **2**, 780 (2007)

D. Di Carlo, L.P. Lee, Anal. Chem. **78**, 7918 (2006)

D. Di Carlo, H. T. K. Tse, and D. R. Gossett, in Single-cell anal. Methods Protoc., ed. by S. Lindström and H. Andersson-Svahn (Humana Press, Totowa, 2012), pp. 1–10

B. Dorvel, B. Reddy, I. Block, P. Mathias, S.E. Clare, B. Cunningham, D.E. Bergstrom, R. Bashir, Adv. Funct. Mater. **20**, 87 (2010)

E. Evans, A. Yeung, Biophys. J. **56**, 151 (1989)

M. Godin, F.F. Delgado, S. Son, W.H. Grover, A.K. Bryan, A. Tzur, P. Jorgensen, K. Payer, A.D. Grossman, M.W. Kirschner, S.R. Manalis, Nat Meth **7**, 387 (2010)

J. Guck, S. Schinkinger, B. Lincoln, F. Wottawah, S. Ebert, M. Romeyke, D. Lenz, H.M. Erickson, R. Ananthakrishnan, D. Mitchell, J. Käs, S. Ulvick, C. Bilby, Biophys. J. **88**, 3689 (2016)

D. Hanahan, R.A. Weinberg, Cell **100**, 57 (2000)

D. Hanahan, R.A. Weinberg, Cell **144**, 646 (2011)

R.M. Hochmuth, J. Biomech. **33**, 15 (2016)

C. Hou, W. Zuo, M.E. Moses, W.H. Woodruff, J.H. Brown, G.B. West, Science **322**, 736 (2008)

T.G. Kuznetsova, M.N. Starodubtseva, N.I. Yegorenkov, S.A. Chizhik, Micron **38**, 824 (2007)

J. Li, C. Thielemann, U. Reuning, D. Johannsmann, Biosens. Bioelectron. **20**, 1333 (2005)

A.C. Lloyd, Cell **154**, 1194 (2013)

H. Lodish, A. Berk, P. Matsudaira, C.A. Kaiser, M. Krieger, M.P. Scott, S.L. Zipursky, J. Darnell, *Molecular Cell Biology*, 5th edn. (WH Freeman, New York, 2003)

L.J. Millet, E.A. Corbin, R. Free, K. Park, H. Kong, W.P. King, R. Bashir, Small **8**, 2555 (2012)

J. Mitchison, Int. Rev. Cytol. **165** (2003)

J.M. Mitchison, Theor. Biol. Med. Model. **2**, 4 (2005)

K. Park, L.J. Millet, N. Kim, H. Li, X. Jin, G. Popescu, N.R. Aluru, K.J. Hsia, R. Bashir, Proc. Natl. Acad. Sci. **107**, 20691 (2010)

K. Park, A. Mehrnezhad, E.A. Corbin, R. Bashir, Lab Chip **15**, 3460 (2015)

M. Plodinec, M. Loparic, C.A. Monnier, E.C. Obermann, R. Zanetti-Dallenbach, P. Oertle, J.T. Hyotyla, U. Aebi, M. Bentires-Alj, L.Y.H., C.-A. Schoenenberger, Nat Nano **7**, 757 (2012)

G. Popescu, Y. Park, N. Lue, C. Best-Popescu, L. Deflores, R.R. Dasari, M.S. Feld, K. Badizadegan, Am. J. Physiol.-Cell Physiol **295**, C538 (2008)

G. Popescu, K. Park, M. Mir, R. Bashir, Lab Chip **14**, 646 (2014)

M. Sato, N. Ohshima, R.M. Nerem, J. Biomech. **29**, 461 (2016)

S. Son, A. Tzur, Y. Weng, P. Jorgensen, J. Kim, M.W. Kirschner, S.R. Manalis, Nat. Methods **9**, 910 (2012)

A. Tzur, R. Kafri, V.S. LeBleu, G. Lahav, M.W. Kirschner, Science **325**, 167 LP (2009)

J.H.C. Wang, B.P. Thampatty, *An Introductory Review of Cell Mechanobiology, Biomechanics and Modeling in Mechanobiology* (2006), pp. 1–16

R.A. Weinberg, *The biology of cancer*, 1st edn. (Garland Science, New York, 2006)

D. Wirtz, K. Konstantopoulos, P.C. Searson, Nat. Rev. Cancer **11**, 512 (2011)

J. Yeom, M.A. Shannon, Adv. Funct. Mater. **20**, 289 (2010)

T.A. Zangle, M.A. Teitell, Nat Meth **11**, 1221 (2014)